Catalysis Today xxx (xxxx) xxx–xxx

Contents lists available at ScienceDirect

Catalysis Today

journal homepage: www.elsevier.com/locate/cattod

Janus amphiphilic carbon nanotubes as Pickering interfacial catalysts for the treatment of oily wastewater by selective oxidation with hydrogen peroxide

Jose L. Diaz de Tuesta[a], Bruno F. Machado[b], Philippe Serp[c], Adrián M. T. Silva[b], Joaquim L. Faria[b], Helder T. Gomes[a,b,*]

[a] Centro de Investigação de Montanha (CIMO), Instituto Politécnico de Bragança, Campus de Santa Apolónia, 5300-253 Bragança, Portugal
[b] Laboratory of Separation and Reaction Engineering — Laboratory of Catalysis and Materials (LSRE-LCM), Faculdade de Engenharia, Universidade do Porto, Rua Dr. Roberto Frias, 4200-465 Porto, Portugal
[c] Laboratoire de Chimie de Coordination UPR CNRS 8241 composante ENSIACET, Université de Toulouse, UPS-INP-LCC 4 allé Emile Monso BP 44362, 31030 Toulouse Cedex 4, France

ARTICLE INFO

Keywords:
Janus
Carbon nanotubes
Oily wastewater
Amphiphilic catalysts
CWPO
Biphasic oxidation
Lipophilic pollutant

ABSTRACT

Janus-like amphiphilic carbon nanotubes (CNTs) were tested as catalysts in the oxidation of 2-nitrophenol (2-NP) with hydrogen peroxide. A biphasic oil-water medium was used to simulate oily wastewater contaminated with the lipophilic model pollutant 2-NP. The CNTs were synthesized by sequentially feeding ethylene and/or acetonitrile, used as carbon and carbon/nitrogen precursors, respectively. The results obtained for 2-NP removal using biphasic systems were compared with those obtained by CWPO using aqueous solutions. The most active catalyst in the CWPO of 2-NP in aqueous solution was the CNT synthesized only with ethylene. This was explained by its high lipophilic character, allowing the complete removal of 2NP after 24 h of reaction at 50 °C, pH_0 = 3, C_{cat} = 0.25 g L^{-1}, $C_{2\text{-}NP,0}$ = 0.5 g L^{-1} and the stoichiometric quantity of H_2O_2 needed for the total mineralization of 2-NP. For the oxidation of 2-NP in biphasic medium, only the Janus-like amphiphilic CNTs (containing a lipophilic undoped section synthetized from ethylene and a hydrophilic N-doped section synthetized from acetonitrile) revealed catalytic activity for the removal of 2-NP. The conversion of 2NP reached in biphasic oxidation conditions was 76.7% after 24 h of reaction at 50 °C, considering pH_0 = 3, C_{cat} = 2.27 g L^{-1} of total volume (water/oil ratio of 16:50 v/v) and $C_{2\text{-}NP,oil,0}$ = 5 g L^{-1}. This removal was ascribed to the formation of Pickering emulsions, by maximizing the interfacial area through an increased contact between the catalyst and both liquid phases. A kinetic model is proposed to accurately predict the experimental data and evaluate the rate constants of the process and its variation with the prepared CNTs.

1. Introduction

Industrial development is leading to an increase in the amount of oily products used and, in spite of technical and management improvements, among other reasons, a great amount of oily compounds are transferred into water bodies, causing pollution. The need to treat oily wastewater sources is becoming increasingly important, since oil industry, oil refining, oil storage, transportation and petrochemical industries generate high volumes of oily wastewater [1–4]. These streams are considered contaminated due to the presence of water and undesired organic pollutants affecting the quality of the oily product (*e.g.*, contaminated diesel). In this sense, the removal of organic pollutants found in the oil fraction of oily wastewaters is interesting, not only to avoid environmental pollution, but also to recover the otherwise discarded oil phase, which can be a fuel, a lubricant or another potential organic raw material. For this reason, increasing attention is being directed to the development of techniques aiming to the recovery and reuse of valuable oily content in oily wastewaters, such as in cutting fluid oily wastewater [5]. Moreover, stricter legislation has been implemented all over the world to limit the content of sulfur and nitrogen in petroleum fuels, due to the pollution caused by its combustion since S- or N- containing molecules can form SO_x and NO_x. Thus, the development of new technologies to deeply remove S and N compounds from oily products is also important in the field of fossil fuels [6].

In our previous study, the adsorption of Sudan-IV, selected as a model lipophilic pollutant, was assessed using modified activated carbons [7]. However, adsorption is not a destructive technique and an additional treatment is necessary to remove the pollutant from the

* Corresponding author.
E-mail address: htgomes@ipb.pt (H. T. Gomes).

https://doi.org/10.1016/j.cattod.2019.07.012
Received 15 February 2019; Received in revised form 4 July 2019; Accepted 10 July 2019
0920-5861/

adsorbent. In this regard, catalytic wet peroxide oxidation (CWPO) appears as an advantageous alternative for the treatment of pollutants from oily wastewater, if proper catalysts are designed for this purpose. CWPO has been explored using different carbon-based materials as catalysts, such as carbon black, activated carbons, glycerol-based carbon materials, carbon xerogels and carbon nanotubes (CNTs) [8–12]. In these studies, phenol, 4-nitrophenol (4-NP) and 2-nitrophenol (2NP) were used as model pollutants in aqueous phase, due to their well-known hazardous properties. In particular, nitrophenols (NPs) are contaminants commonly present in wastewaters of plastic, pharmaceutical, pesticide, synthetic dyes, and explosive industries, reaching high concentrations in these effluents [13,14]. NPs are highly toxic, inhibitory and bio-refractory organic compounds [15,16]. The United States Environmental Protection Agency has included NPs in the list of priority pollutants [17], and limited their maximum allowable concentration in water to 20 ppb [18]. NPs are also highly lipophilic [19], and thus, they can be found in higher concentrations in oily phases than in aqueous ones when present in liquid–liquid (L–L) biphasic mixtures. Abraham et al. has reported the partition coefficient, measured as log*P*, of different NPs in octanol-water, 1,2-dichloroethane-water and cyclohexane-water, as 1.79, 2.81 and 1.51 for 2-NP, respectively, which was more lipophilic than phenol, 3-NP, 4-NP, 2,3-NP and 2,4-NP [19].

In particular, CNTs were evaluated in the CWPO of 4-NP, revealing high catalytic activity [12]. These materials were synthesized by catalytic chemical vapor deposition (CVD), feeding sequentially ethylene and acetonitrile, as carbon and carbon/nitrogen precursors, respectively, leading to amphiphilic CNTs with a double structure, similar to that found in Janus particles [20]. A Janus-like material contains two sections with different surface chemistries [21], making the material useful for various applications [22,23]. In this sense, these solid materials can act as emulsifiers, allowing oil-aqueous emulsions to be stabilized with macroscopic solid particles, known as Pickering emulsions [24]. In addition, materials can also act as catalyst on processes occurring in biphasic L-L mixtures, *i.e.* as Pickering Interfacial Catalysts (PIC), which are able to participate simultaneously as emulsifier and catalysts [24]. Thus, Janus particles are very suitable for the treatment of oily wastewater contaminated with lipophilic pollutants. Catalysts with these properties can promote reactions at the LL interface by increasing the contact between both phases (maximizing the interfacial area) and ensuring a higher mass transfer of the pollutants between these phases. It should be noted that the oxidation of lipophilic pollutants present in an oily wastewater with hydrogen peroxide leads to more hydrophilic products, enhancing their transfer to the aqueous phase, thus cleaning the oil phase [6,25].

The current work deals with the removal of 2-NP, used as a lipophilic model pollutant, from a biphasic oil-water medium (simulating contaminated oily wastewater effluents) by its oxidation with hydrogen peroxide employing amphiphilic Janus-like CNTs. In addition, a kinetic model is proposed to accurately predict the experimental data and evaluate the rate constants of the process and its variation with the prepared CNTs. To the best of our knowledge, there are no studies regarding the kinetic modelling of the oxidation of an organic compound in an emulsified biphasic mixture with carbon nanotubes.

2. Materials and methods

2.1. Reagents

The reactants involved in the oxidation runs were 2-NP (98 wt%) and H_2O_2 (30%, w/v), provided by Sigma-Aldrich and Fluka, respectively. Cyclochexane (99.99%), used as oil phase in the biphasic system, was obtained from Fisher Chemical. Cyclohexanol (99%) and cyclohexanone (99.6%) were obtained from Alfa Aesar and Aldrich, respectively. Titanium (IV) oxysulfate ($TiOSO_4$, 15 wt.% in dilute sulfuric acid, H_2SO_4 99.99%), hydrochloric acid (HCl, 37 wt.%) and sodium sulfite (Na_2SO_3, 98 wt.%) were purchased from Sigma-Aldrich. Sodium hydroxide (NaOH, 98 wt.%) was obtained from Panreac. The mobile phase used in HPLC analyses was composed of methanol (HPLC grade), glacial acetic acid (analytical reagent grade) and acetonitrile (99.99%), available from Fisher Chemical. All chemicals were used as received without further purification. Distilled water was used throughout the work. $Fe(NO_3)_3$ (≥98%) and γ-Al_2O_3 (SCCa 5/150, S_{BET} = 172 $m^2\,g^{-1}$), used for the preparation of the CNT catalysts, were acquired from Sigma-Aldrich and Sasol, respectively. The acetonitrile (99.5%) used in the synthesis of the CNTs was obtained from Sigma-Aldrich, whereas nitrogen (N50), ethylene (N25) and hydrogen (N55) gases were supplied by Air Liquide.

2.2. Synthesis of CNTs

The CNTs were synthesized by CVD in a fluidized-bed reactor using ethylene and acetonitrile as carbon and nitrogen/carbon sources, respectively, according to the procedure described elsewhere [12,20]. The CVD synthesis was conducted by employing Fe/γ-Al_2O_3 (20 wt.% Fe) as catalyst, prepared by incipient impregnation using an aqueous solution of $Fe(NO_3)_3$ onto the surface of γ-Al_2O_3. The Fe-containing catalyst was pre-reduced *in situ* using 40 vol.% H_2 (in N_2) for 30 min at 650 °C, before the CVD growth was carried out using a gas mixture with 45% N_2/30% H_2/25% C_2H_4 for the CNT carbon composed section, and with 60% N_2/40% H_2 bubbling through an acetonitrile solution at 35 °C for the N-CNT section. Five different samples were produced by feeding sequentially the fluidized bed reactor with ethylene and/or acetonitrile during the following periods: (1) C_2H_4 for 30 min; (2) C_2H_3N for 20 min, followed by C_2H_4 for 20 min; (3) C_2H_4 for 10 min, followed by C_2H_3N for 20 min; (4) C_2H_3N for 20 min, followed by C_2H_4 for 10 min; and (5) C_2H_3N for 30 min; resulting in E30, A20E20, E10A20, A20E10 and A30 samples, respectively. Finally, the synthesized CNTs were purified under reflux at 140 °C in an aqueous solution of H_2SO_4 (50 vol. %) for 3 h, to facilitate the total dissolution of the alumina and exposed Fe particles.

2.3. Characterization techniques

Thermogravimetric analyses (TGA) were conducted under air in a Diamond TG/DTA (PerkinElmer Inc.) apparatus with a 10 °C min^{-1} ramp between 30 and 1000 °C. The textural properties of the CNTs were determined using N_2 adsorption-desorption isotherms at –196 °C, obtained in a Quantachrome NOVA 4200e adsorption analyser. The specific surface area (S_{BET}) was calculated using the BET method (applied in the range of relative pressure, p/p^0, between 0.05 and 0.15) [26], and the external surface area (S_{ext}) and the micropore volume (V_{mic}) assessed by the *t*-method (thickness was calculated by employing ASTM standard D-6556-01) [27]. The total pore volume (V_{Pore}) was calculated at *ca.* p/p^0 = 0.98. The hydrophobicity/hydrophilicity of the CNTs (in the form of buckypapers) was determined by water contact-angle measurements using an Attension optical tensiometer (model Theta) that allowed image acquisition and data analysis. The measurements with water were performed on dry buckypapers at room temperature using the sessile-drop method. Each contact angle was measured at least in five different locations on the buckypapers to determine the average value. Elemental analysis was performed in a Carlo Erba EA 1108 Elemental Analyser in order to quantify the carbon, hydrogen, nitrogen and sulfur contents. TEM images were obtained using a JEOL 1011 transmission electron microscope operating at 100 kV.

2.4. Oxidation runs

Catalytic oxidation experiments were performed in a stirred 250 mL glass reactor, equipped with a condenser and a temperature measurement thermocouple. In the experiments performed in aqueous media, 50 mL of a 2-NP 500 mg L^{-1} solution was first loaded to the reactor and

then heated to 50 °C by immersion of the reactor in an oil bath at controlled temperature. Upon stabilization at the desired temperature, the solution pH was adjusted to the initial pH (pH_0) of 3 using H_2SO_4 and NaOH solutions, and the experiments proceeded freely (*i.e.*, not buffered), without further pH adjustment. Then, CNT sample (0.25 g L^{-1}) was loaded to the aqueous solution and a calculated volume of a 30% w/v H_2O_2 solution was added in order to use the stoichiometric dosage of H_2O_2 needed for complete 2-NP mineralization. That moment was considered as the initial reaction time, t_0 = 0 min.

The experiments in biphasic systems were performed under similar conditions (50 °C, pH_0 = 3 and stoichiometric amount of H_2O_2 needed for a complete 2-NP mineralization), but with volumes of 16 and 50 mL respectively for the aqueous and oily (cyclohexane) phases, maintaining the proportions considered in a previous work [20]. In these runs, 2NP was added in order to achieve a theoretical concentration of 5 g L^{-1} in the oil phase and as a result, the catalyst load was also increased, not only to maintain a similar 2-NP/catalyst ratio, but also to add the amount necessary to establish a Pickering emulsion, as reported elsewhere [20]. The initial concentration in the two phases was then established by the partition coefficient of 2-NP between both phases (P_{OW} = 1.52 in a cyclohexane-water mixture, [19]). During the first 10 min of reaction, the medium was sonicated to stabilize the emulsion (minimum time required for the stabilization of emulsions with other carbon materials [22,23]). The sonication procedure was performed for all runs, even in those carried out under not emulsified mixtures in order to take into account possible interferences. All the experiments (oxidation runs performed in both aqueous and L-L biphasic systems) were conducted during 24 h and monitored by taking several samples from the reactor at previously selected times of reaction. The aliquots were centrifuged to break the emulsion and separate the solid catalyst from the liquid phases.

Selected experiments were performed in triplicate, in order to assess reproducibility and error of the experimental results. Additionally, adsorption experiments of 2-NP on CNTs were also performed in aqueous solutions and in L-L biphasic media under the same operating conditions as those used in the reaction runs (50 °C, pH_0 = 3, 500 mg L^{-1} of 2-NP in water and 5 g L^{-1} of 2-NP in oil and the corresponding catalyst load) in order to compare with the removal of 2-NP obtained in catalytic runs.

2.5. Analysis of aqueous and oil samples

The liquid phase samples withdrawn from the reactor were analyzed by HPLC and using a colorimetric method, as previously described [10–12]. Briefly, 2-NP and its possible aromatic oxidation products (in particular catechol and phenol), were identified using a Jasco HPLC system at a wavelength of 277 nm (UV-2075 Plus detector). A Kromasil 100-5-C18 column was used as stationary phase feeding as eluent 1 mL min^{-1} (PU-2089 Plus) of an A:B (40:60) mixture containing (A) 3% acetic acid and 1% acetonitrile in methanol and (B) 3% acetic acid in ultrapure water. In order to determine the concentration of H_2O_2, a filtered sample was added to 1 mL of H_2SO_4 solution (0.5 mol L^{-1}) in a 20 mL volumetric flask, to which 0.1 mL of $TiOSO_4$ was added. The resulting mixture was diluted with distilled water and further analyzed by UV–Vis spectrophotometry (T70 spectrometer, PG Instruments Ltd.) at a wavelength of 405 nm.

The oily phase was analyzed by GC-FID (Scion 436-GC from Bruker) to determine the concentration of 2-NP, aromatic intermediate products resulting from its oxidation, as well as to evaluate the oxidation of cyclohexane, following the evolution of cyclohexanol and cyclohexanone. With this purpose, aliquots were prepared without further derivation, but small quantities of Na_2SO_3 were added to remove moisture. The injector and detector temperatures were set to 260 and 270 °C, respectively. Complete separation of the compounds was achieved on a 50 m x0.25 mm CP-Sil 88 chromatography column using the following oven temperature program: a first isothermal step at 160 °C during 5 min, followed by a heating ramp of 5 °C min^{-1} to 170 °C, then 10 °C min^{-1} until 220 °C and a final isothermal step for 5 min.

2.6. Kinetic modelling

A kinetic study of the oxidation runs performed in aqueous solutions was carried out following the methodology considered in a previous work regarding the CWPO of phenol [8]. The disappearance rate of each specie i ($-r_i$, in mmol h^{-1} g^{-1}) inside the batch-reactor was expressed as given in Eq. 1.

$$-r_i = \frac{1}{W_{cat}} \cdot \frac{dN_i}{dt} \tag{1}$$

where N_i and W_{cat} are the moles of compound i (mmol) and the catalyst load (g) in the reactor, respectively, and t is the time of reaction (h). For the runs performed in aqueous solutions, the rate was expressed considering a single system with constant volume, as shown in Eq. 2.

$$-r_i = \frac{1}{W_{cat}} \cdot \frac{dN_i}{dt} = \frac{1}{C_{cat}} \cdot \frac{dC_i}{dt} \tag{2}$$

where C_i and C_{cat} are the corresponding concentrations of the compound i (mM) and the catalyst (g L^{-1}), respectively.

The same methodology was followed to model the biphasic oxidation mixture containing cyclohexane and water. In this system, the volume was considered constant in each phase and the species expressed in their concentrations in both oil and water phases.

The rate equations were solved and the kinetic parameters were obtained using a numerical integration minimizing the sum of squared errors (SSE_{model}) of the relative concentration of each compound i ($rc_i = C_i/C_{i,0}$) between the experimental (*exp*) and the predicted (*model*) values, as given in Eq. 3.

$$SSE_{model} = \sum_{n=1}^{N} (rc_{exp\,i,n} - rc_{model\,i,n})^2 \tag{3}$$

rc_i was used to take into account the differences in the order of magnitude of the concentrations among the compounds considered ($C_{2\text{-}NP,aq}$ = 0–3.6 mM, $C_{2\text{-}NP,oil}$ = 0–36 mM and $C_{H_2O_2}$ = 0–1.65 M, whereas $C_i/C_{i,0}$ = 0–1 for each compound *i*). Kinetic models were also evaluated by the coefficient of determination (R^2).

3. Results and discussion

3.1. Characterization of the CNTs

The porosity of the materials was assessed using N_2 adsorption-desorption isotherms at –196 ºC, depicted in Fig. 1. As can be observed, all the materials show a low adsorbed N_2 volume at low relative pressure (p/p^0), revealing that the materials contain less micropores (< 2 nm) than activated carbons [7]. On the other hand, at higher relative pressures, a hysteresis loop between the adsorption and the desorption branches is observed. According to the IUPAC classification [28], this N_2 adsorption-desorption isotherm can be classified as Type II with a H3 hysteresis loop, typically found for macroporous materials. In this case, this type of isotherm is likely a consequence of CNT aggregation. All the studied materials show identical adsorption-desorption profiles. The main difference between the materials was the total N_2 adsorption at a relative pressure of 0.98, reaching *ca.* 1100 cm^3 g^{-1} for the E30 sample, whereas *ca.* 650 cm^3 g^{-1} was measured for A30. Materials synthesized using both ethylene and acetonitrile precursors, *viz.* A20E20, E10A20 and A20E10, revealed values of adsorbed volumes ranging between those determined for E30 and A30 (650-1100 cm^3 g^{-1}). The textural properties (S_{BET} and V_{Total}), as well as water contact angles, and elemental analysis of the synthesized carbon materials are summarized in Table 1. Analyzing the isotherms by the *t*-plot method, it was found that the external specific surface area

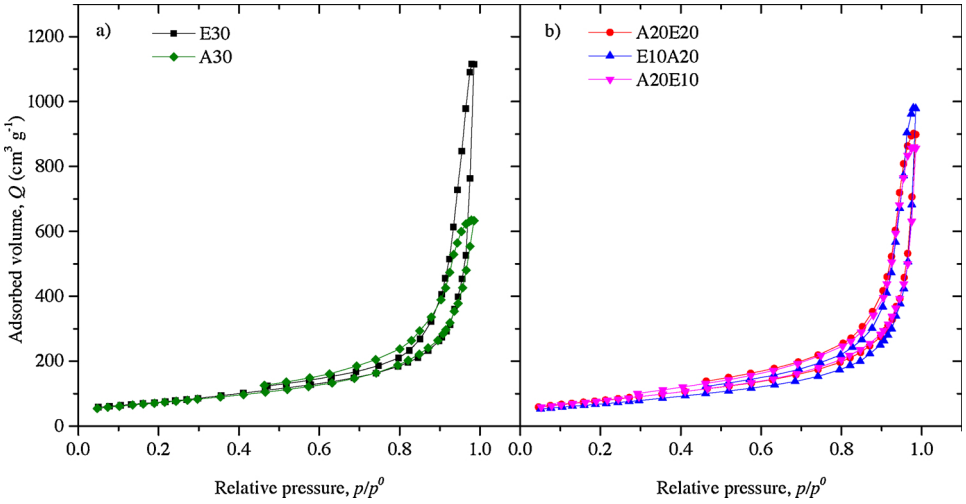

Fig. 1. N_2 Adsorption-desorption isotherms at –196 ºC of (a) E30 and A30; and (b) Janus amphiphilic CNTs.

obtained for each material corresponds to the respective value of its S_{BET}, reported in Table 1, confirming that the materials are not microporous. Additionally, the micropore volume determined by the *t*-plot method was also found to be zero. The BET surface of all samples varies between 245 and 285 $m^2 g^{-1}$, and it is possible to observe a decrease in total pore volume (V_{Total}) as the N-content increases (Table 1), likely due to the larger diameter of the CNTs when acetonitrile is used as a precursor for the CNT growth (Fig. 2). In this regard, V_{Total} increases, and N-content decreases, in the following order: E30 > E10A20 > A20E20 > A20E10 > A30. As expected, the sample synthesized entirely with ethylene does not contain nitrogen. Interestingly, the N-content incorporated in A20E10 (4.5%) and E10A20 (3.2%) is different, despite both ethylene and acetonitrile precursors being fed during the same time in the synthesis procedure. Hence, the N-content in the Janus-structured amphiphilic materials depends significantly on the feeding order of the precursors, reaching higher N-content when acetonitrile is fed first. This is a consequence of the larger growth kinetics (determined through the yield) of undoped CNTs (when using initially ethylene), compared to N-CNTs [20]. In this way, it is possible to control the N-content of the materials by varying the feeding time and the feeding order of each precursor (ethylene for the undoped section and acetonitrile for the N-doped section). Consequently, the hydrophilic character of the materials can be designed for specific applications, as evidenced by the water contact-angle measurements (Table 1). As expected, the hydrophobicity of the samples decreased with their N-content. The maximum amount of N (5.6%) was obtained for the material synthesized only with acetonitrile (A30).

The remaining content obtained after the elemental analysis of the samples, determined as the balance from the CHN-contents, varies between 3.0 and 9.2%. This non−CHN content is typically ascribed to ashes (inorganic content), sulfur and oxygen. The samples were purified with H_2SO_4 (50 vol.%) to remove the exposed Fe/γ-Al_2O_3 catalyst, resulting in samples with a low content of sulfur (< 0.75%). As a consequence of this purification treatment, some defects were introduced on the CNTs (mostly on the tips), which then acted as reactive sites for the formation of oxygen-containing groups. Hence, the non−CHN content can be ascribed mainly to oxygen and Fe/γ-Al_2O_3 catalyst confined in the CNTs. The metal content is higher for the N-doped samples due to the cupstacked or bamboo-like structure of the N-doped CNTs (Fig. 2), since this structure favors the confinement of metal species from the catalyst. As can be observed in the TEM images, the carbon nanotubes synthesized only with ethylene (E30) possess the smallest external diameter (*ca.* 10 nm) and wall thickness (*ca.* 5 nm), whereas the sample synthesized using only acetonitrile (with a bamboo-like structure) has roughly a diameter which is the double of E30. Samples synthesized using both ethylene and acetonitrile precursors (A20E20, E10A20 and A20E10) show both structures (identified in Fig. 2), confirming the synthesis of Janus-structured materials.

The presence of the two structures was also evidenced by the different profiles of mass loss observed during thermogravimetric analyses (Fig. 3). Samples synthesized with a single precursor (with only ethylene or acetonitrile) showed a homogeneous mass loss centered at 585 ± 5 and 435 ± 5 °C (from the derivative of mass loss profile represented in gray) for materials E30 and A30, respectively. These results reveal a greater stability of the sample E30 when compared to A30. In the case of the Janus-structure amphiphilic materials, synthesized with the sequential feed of both ethylene and acetonitrile precursors (A20E20, E10A20 and A20E10), two peaks are observed in the derivatives of the mass loss profiles. These peaks are exactly identified at the same decomposition temperatures found for E30 and A30, putting in evidence the two different structures in the material, the N-doped and the undoped, which yield materials with a Janus-like structure. Thus, these materials can be used as Pickering emulsifiers (emulsions stabilized by solid particles).

3.2. CWPO of 2-NP in aqueous phase

Fig. 4 shows the conversion of both H_2O_2 and 2-NP in the CWPO, as well as the removal of 2-NP obtained in the adsorption runs, that were carried out in the presence of each synthesized CNT after 24 h. As can be

Table 1
Textural properties, water contact angles (θ) and elemental analysis composition of the synthesized CNTs.

Sample	S_{BET} ($m^2 g^{-1}$)	V_{Total} ($cm^3 g^{-1}$)	C (%)	H (%)	N (%)	Remaining (%)	θ (º)
E30	264	1.72	97.0	0.0	0.0	3.0	60 ± 2
E10A20	245	1.51	90.7	0.0	3.2	6.1	47 ± 2
A20E20	285	1.39	91.0	0.0	3.3	5.7	24 ± 1
A20E10	283	1.32	88.4	0.1	4.5	7.0	21 ± 1
A30	258	0.97	84.7	0.5	5.6	9.2	11 ± 1

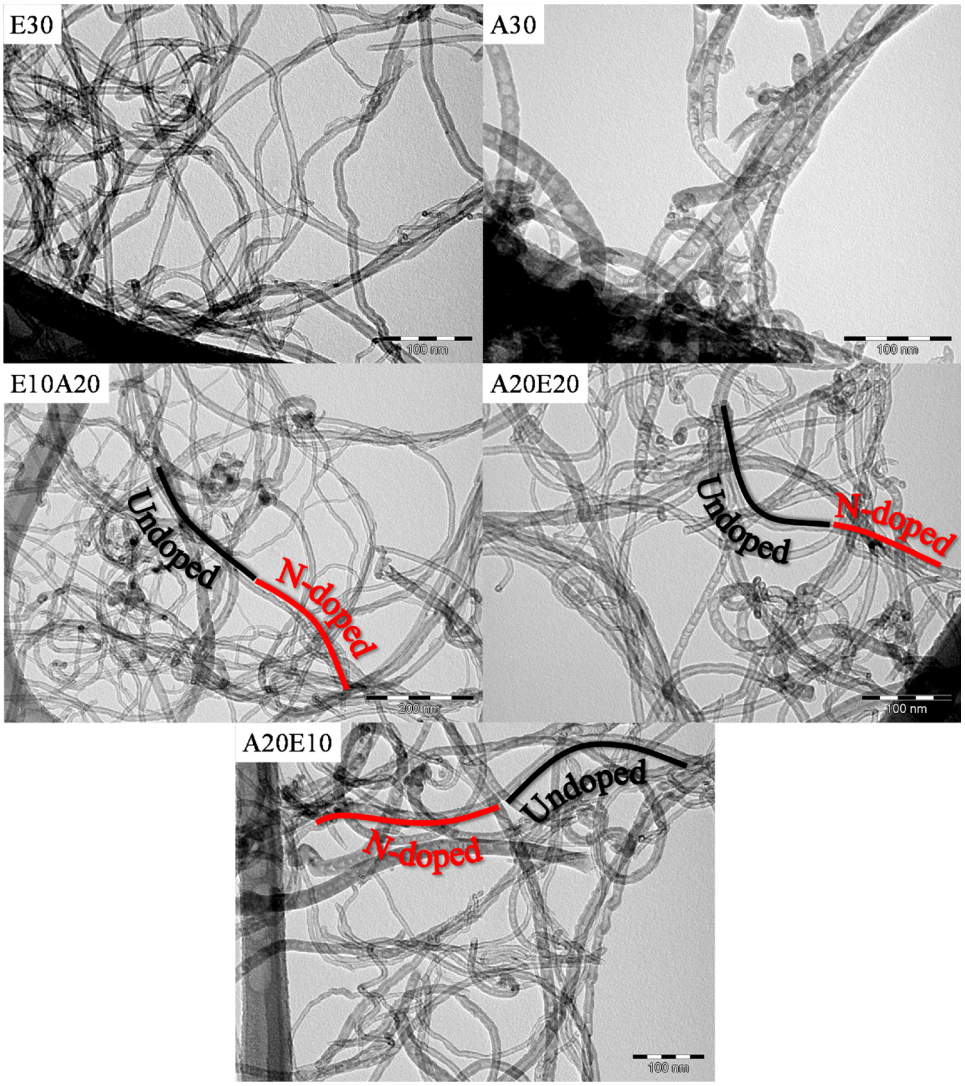

Fig. 2. TEM images of the synthesized CNTs.

observed, all tested materials show catalytic activity in the CWPO of 2-NP, since the conversions of both H_2O_2 and 2-NP are higher in presence of the catalysts than in the non-catalytic run ($X_{H_2O_2}$,CWPO = 13.1% and $X_{2\text{-}NP,CWPO}$ = 13.2%). In addition, the conversions of 2-NP obtained in the CWPO runs ($X_{2\text{-}NP,CWPO}$ > 14.8%) are always higher than the removal achieved in the adsorption experiments for each CNT ($X_{2\text{-}NP,Ads.}$ < 13.0%). The highest removal of 2-NP by adsorption (13.0%) was obtained for the sample E30, whose amount of adsorbed 2-NP per gram of CNT was q_e = 21.7 mg g^{-1}. It should be noted that the adsorbed amount of 2-NP on all samples decreases in the same order as the total pore volume, determined by analysis of the N_2 adsorption-desorption isotherms at –196 ºC, namely: E30 > E10A20 (q_e = 20.2 mg g^{-1}) > A20E20 (q_e = 18.1 mg g^{-1}) > A20E10 (q_e = 15.0 mg g^{-1}) > A30 (q_e = 11.7 mg g^{-1}). The removal of 2-NP by CWPO also reaches the highest value for the sample E30, and the same decrease order is observed: E30 ($X_{2\text{-}NP,CWPO}$ > 99.9%) > E10A20 ($X_{2\text{-}NP,CWPO}$ = 87.8%) > A20E20 ($X_{2\text{-}NP,CWPO}$ = 85.7%) > A20E10 ($X_{2\text{-}NP,CWPO}$ = 34.6%) > A30 ($X_{2\text{-}NP,CWPO}$ = 14.8%). On the other hand, the conversion of H_2O_2 follows approximately the inverse order, the same order as decreasing N-content in the samples: A30 ($X_{H_2O_2}$,CWPO = 98.0%) > A20E10 ($X_{H_2O_2}$,CWPO = 88.7%) > E10A20 ($X_{H_2O_2}$,CWPO = 66.2%) > A20E20 ($X_{H_2O_2}$,CWPO = 55.2%) > E30 ($X_{H_2O_2}$,CWPO = 49.7%). This means that higher N-contents, corresponding to materials with lower hydrophobic character, lead to higher conversions of hydrogen peroxide and lower removal of 2-NP.

Although ethylene and acetonitrile were fed during the same time (10 and 20 min, respectively) to synthesize E10A20 and A20E10, their catalytic activities are rather different, 2-NP removals of 87.8 and 34.6% being obtained, respectively, by CWPO. This was ascribed to the different order of feeding of the ethylene and acetonitrile precursors during their synthesis, leading to materials with distinct physico-chemical properties, such as the N-content and water contact angles (Table 1).

Similar trends regarding the influence of N-content in the pollutant and H_2O_2 conversions were also observed in a previous work regarding the CWPO of 4-NP as model pollutant with CNTs synthesized using ethylene and acetonitrile with different feeding times [12]. In that work, similar conversions of 4-NP were achieved when compared to the conversions of the 2-NP obtained in this work under similar operating conditions.

When comparing the results obtained in this work with those reported in previous works regarding the CWPO of 2-NP, the conversion of 2-NP reached with the material E30 is much higher ($X_{2\text{-}NP,CWPO}$ > 99.9% after 24 h) than that obtained with activated carbons ($X_{2\text{-}NP,CWPO}$ < 35% after 24 h), glycerol-based carbon materials ($X_{2\text{-}NP,CWPO}$ ≈ 60% after 24 h) and with carbon xerogels ($X_{2\text{-}NP,CWPO}$ ≈ 20% after 24 h) under similar operating conditions ($C_{2\text{-}NP,0}$ = 0.1 g L^{-1}, $C_{H_2O_2}$,0 = 34.6 mM, C_{cat} = 0.1 g L^{-1}, pH_0 3 and 50 °C) [10]. At identical concentrations ($C_{2\text{-}NP,0}$ = 0.5 g L^{-1}, $C_{H_2O_2}$,0 = 52.2 mM,

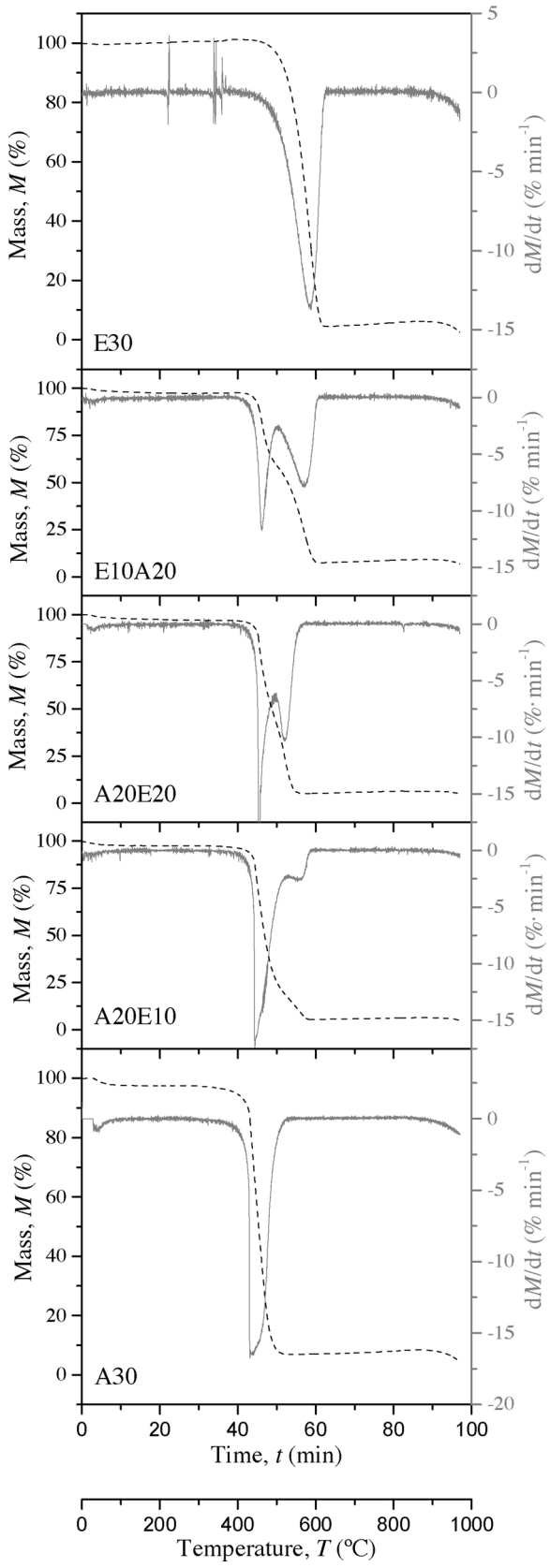

Fig. 3. Weight loss (black dashed line) and corresponding first derivative (gray line) of the CNTs obtained by TGA.

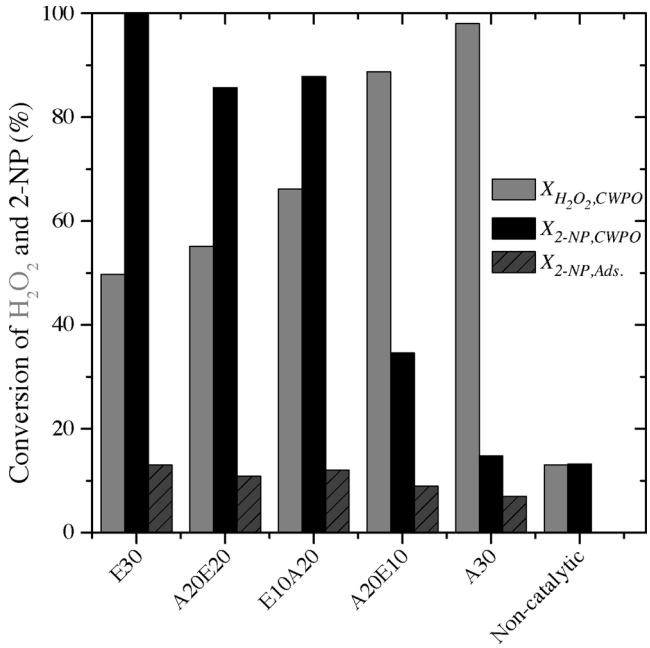

Fig. 4. Conversion of hydrogen peroxide ($X_{H_2O_2}$,CWPO) and 2-NP ($X_{2\text{-}NP,CWPO}$) in CWPO and the removal of 2-NP ($X_{2\text{-}NP,Ads.}$) by adsorption carried out with the synthesized CNTs in aqueous phase after 24 h. Operating conditions: 50 °C, pH_0 = 3, C_{cat} = 0.25 g L^{-1}, $C_{2\text{-}NP,0}$ = 0.5 g L^{-1} and stoichiometric quantity of H_2O_2 needed for the total mineralization of 2-NP (or CWPO experience).

C_{cat} = 0.25 g L^{-1}) to those used in this study, the highest conversion of 2-NP obtained by CWPO with glycerol-based carbon materials was also lower ($X_{2\text{-}NP,CWPO}$ ≈ 80% after 24 h) than that achieved with the sample E30 [11].

The results obtained in the CWPO of 2-NP in aqueous phase reveal the potential of the synthesized CNTs for CWPO processes.

3.3. Oxidation of 2-NP in a biphasic L–L mixture

3.3.1. Emulsion and mass transfer

The ability of the CNTs to act as Pickering emulsifiers was tested in the stabilization of a water-cyclohexane biphasic mixture with a volume ratio of 16:50 mL/mL and a CNT load of 150 mg, as reported elsewhere [20]. The experiments were performed under the operating conditions of the CWPO runs (50 °C and pH_0 = 3). The emulsion stabilization of the mixtures was not achieved by fast stirring, but it was achieved under sonication, as shown in Fig. S1. The sonication was applied during 10 min in order to assure the stabilization of the emulsion [22,23]. CNTs synthesized with both acetonitrile and ethylene precursors (A20E20, E10A20 and A20E10) formed perfectly stable Pickering emulsions as schematized in Fig. 5a, maintained during 48 h. However, CNTs prepared with acetonitrile (hydrophilic A30) or with ethylene only (lipophilic E30) are not capable of forming emulsions. The presence of the oxidant (H_2O_2) was assessed and it did not affect the emulsions stabilized by the CNTs.

The mass transfer of 2-NP at the interface of the L–L biphasic mixture of cyclohexane and water was also evaluated, since it is crucial for the process performance, as represented in Fig. 5b. For this purpose, 50 mL of a 5 g L^{-1} 2-NP cyclohexane solution was added to 16 mL of distilled water (W/O = 16:50) under strong stirring at the reaction operating conditions (50 °C and pH_0 = 3). The transfer of 2-NP occurred very fast, as 99.9% of 2-NP in the aqueous phase achieved the equilibrium in less than 5 min. This equilibrium is established by the partition coefficient of 2-NP in the biphasic mixture of water-cyclohexane, defined as the ratio between the concentration of 2-NP in oil and in water, which was 32.4 under the operating conditions cited above. The

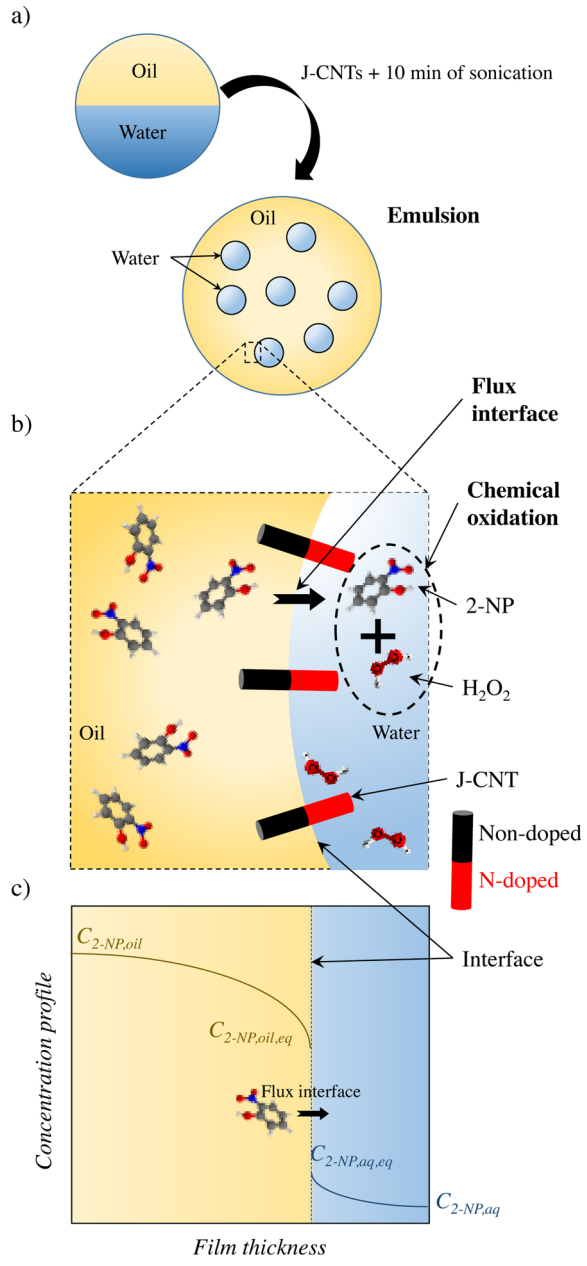

Fig. 5. Schematic representation of (a) emulsion stabilization, (b) mass transfer of 2-NP and its oxidation close to the interface and (c) concentration profile of 2-NP in both oil and water phases close to the interface stabilized by the synthesized CNTs.

concentration of 2-NP in cyclohexane and in water at those experimental conditions (16:50 mL/mL, 50 °C and pH_0 = 3) is 4.86 and 0.15 g L^{-1}, respectively, at the equilibrium. The partition coefficient was similar to the values 32.4–34.7 reported in the literature [19]. The mass transfer rate of 2-NP between the phases in the presence of the CNTs was not possible to measure under the same operating conditions, since the stabilization of the emulsion under sonication requires more time than that needed for the 2-NP transfer. However, experiments in the absence of H_2O_2 did allow to conclude that the partition coefficient of 2-NP was not significantly affected by the presence of the CNTs.

3.3.2. Oxidation runs

The concentration decay curves of H_2O_2 and 2-NP in the aqueous and organic phases during the oxidation runs performed in the biphasic mixture of cyclohexane and water are depicted in Fig. 6. The conversion

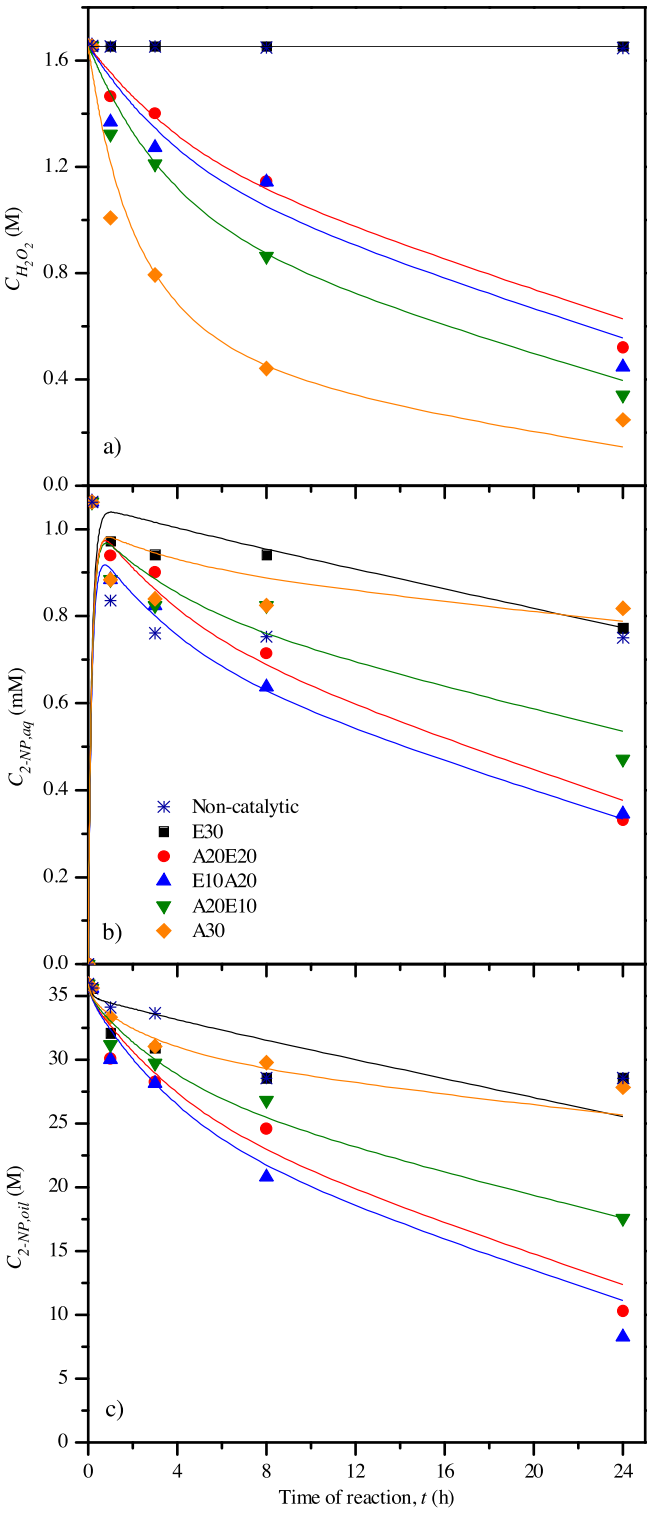

Fig. 6. Evolution of the concentration of (a) H_2O_2, (b) 2-NP in aqueous phase and (c) 2-NP in oil phase during CWPO experiments (symbols represent the experimental data whereas the lines represent the values predicted by the kinetic model, Eqs. 14, 18 and 22). Operating conditions: 50 °C, W/O = 16:50 (v/v), pH_0 = 3, C_{cat} = 2.27 g L^{-1} of total volume, $C_{2\text{-}NP,oil,0}$ = 5.0 g L^{-1} and stoichiometric quantity of H_2O_2 needed for the total mineralization of 2-NP.

of H_2O_2 and 2-NP, calculated from the concentration of 2-NP in both water and oil phases, after 24 h of reaction, is given in Fig. 7. As can be observed, only the amphiphilic materials (A20E20, E10A20 and A20E10) demonstrate significant catalytic activity in the removal of 2-

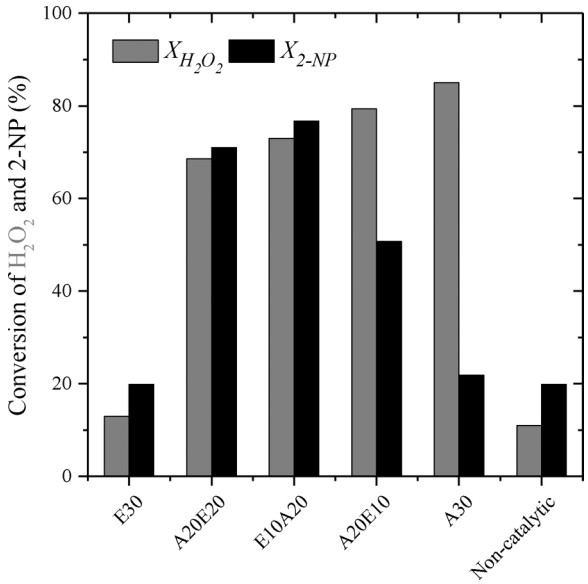

Fig. 7. Conversion of hydrogen peroxide ($X_{H_2O_2}$) and 2-NP ($X_{2\text{-}NP}$) in the CWPO of 2-NP performed in biphasic water-cyclohexane mixtures with CNTs after 24 h. Operating conditions: 50 °C, W/O = 16:50 (v/v), pH_0 = 3, C_{cat} = 2.27 g L^{-1} of total volume, $C_{2\text{-}NP,0,oil}$ = 5 g L^{-1} and stoichiometric quantity of H_2O_2 needed for the total mineralization of 2-NP.

NP ($X_{2\text{-}NP}$ > 50%). This activity can be attributed to the ability of these materials to form and stabilize Pickering emulsions, allowing the contact between the catalyst and both phases, maximizing the interfacial area and ensuring a higher mass transfer between phases. These emulsions also lead to increased hydrogen peroxide decomposition at the interface (especially in the more hydrophilic material section), where 2-NP has its maximum concentration in the aqueous phase, as represented in Fig. 5.

Interestingly, the most active catalytic material in the CWPO of 2-NP in aqueous phase (E30) shows the lowest catalytic activity in the CWPO of 2-NP in the cyclohexane-water biphasic mixture, yielding similar oxidant and pollutant conversions to those obtained in the non-catalytic test ($X_{2\text{-}NP}$ < 20% and $X_{H_2O_2}$ < 15%). The absence of catalytic activity of the E30 material in the biphasic system can be explained by its lipophilic character, thus being preferentially distributed through the organic phase and not contributing to the decomposition of hydrogen peroxide. On the other hand, the more hydrophilic material (A30) was preferably distributed over the aqueous phase, leading to high conversions in the decomposition of hydrogen peroxide.

Among the amphiphilic materials with Janus structure (A20E20, E10A20 and A20E10), a similar trend to that found in the CWPO in aqueous phase was observed. Specifically, the material A20E10 (more hydrophilic and with higher nitrogen content), presented the highest conversion of hydrogen peroxide (79.4% after 24 h of reaction). A20E20 and E10A20 materials, which have a similar N-content, show similar conversions of H_2O_2 (68.6 and 72.9%, respectively) and of 2-NP (71.0 and 76.7%, respectively) after 24 h of reaction.

The selective oxidation of the pollutant is crucial in CWPO processes carried out in biphasic mixtures, since the oxidation of the oil phase cannot take place. In this work, cyclohexanol or cyclohexanone were not observed in any oxidation experiment performed; thus, the oxidation of cyclohexane does not take place under the studied operating conditions, and only oxidation of 2-NP occurred in the CWPO runs with the studied CNTs. Furthermore, the adsorption of 2-NP was neglected.

3.4. Kinetic modelling

The rate of disappearance of the main reactants in the CWPO processes studied (2-NP and H_2O_2) has been explored in order to observe the differences between the kinetics of the chemical oxidation in the aqueous phase and in the biphasic mixture of cyclohexane and water.

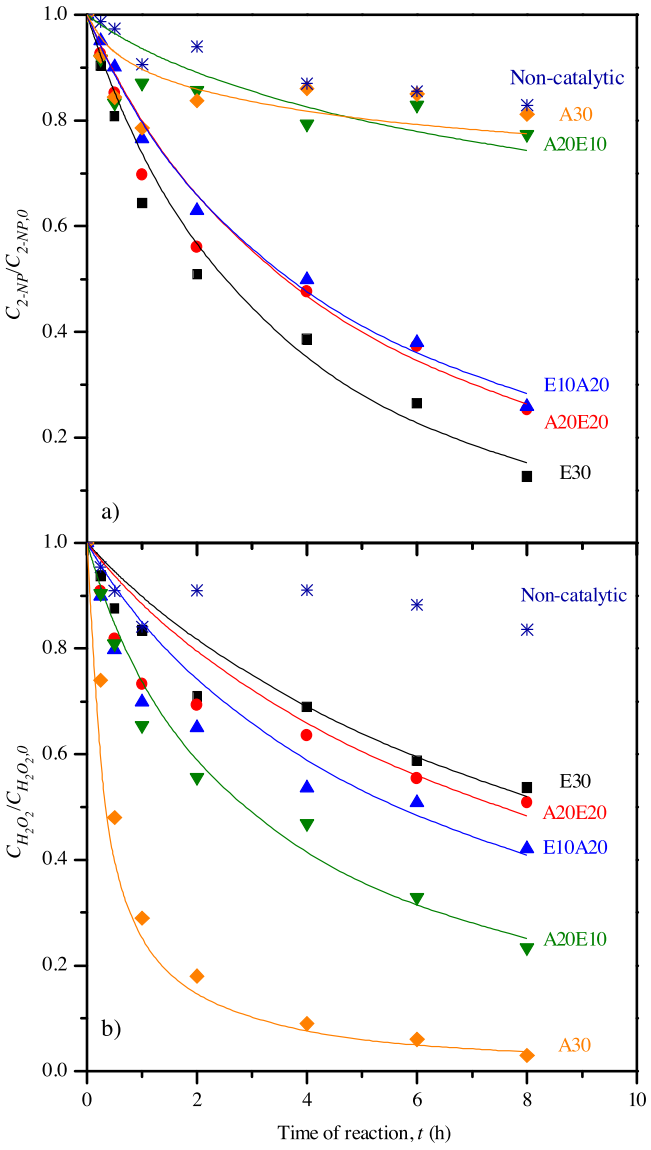

Fig. 8. Evolution of (a) 2-NP and (b) H_2O_2 during the CWPO runs (symbols represent the experimental data whereas the lines represent the values predicted by the kinetic model, Eqs. 8-9). Operating conditions: 50 °C, pH_0 = 3, C_{cat} = 0.25 g L^{-1}, $C_{2\text{-}NP,0}$ = 0.5 g L^{-1} and stoichiometric quantity of H_2O_2 needed for the total mineralization of 2-NP.

3.4.1. CWPO of 2-NP in aqueous solution

Fig. 8 shows the results of H_2O_2 and 2-NP conversion until 8 h of reaction in the CWPO runs of 2-NP in aqueous solution in the presence of each CNT sample. As can be observed, the conversions maintain the same correlation with the N-content (as found in Fig. 4 after 24 h) since the beginning of the reaction. The concentration decay curves of 2-NP and H_2O_2 have been modelled taking into account previous works regarding the CWPO of phenol with carbon materials [8,9]. In this sense, hydrogen peroxide was modelled using a second-order power-law kinetic model, considering that hydrogen peroxide decomposes to hydroxyl and hydroperoxyl radicals at the carbon surface, as given in Eq. 4, and that these radicals further react with the organic matter.

$$2H_2O_2 \rightarrow HO^{\bullet} + HOO^{\bullet} + OH^{-} + H^{+} \quad (4)$$

Thus, the hydrogen peroxide disappearance can be modelled by Eq. 5.

$$-\frac{dC_{H_2O_2}}{dt} = C_{cat}\cdot k_{H_2O_2}\cdot C_{H_2O_2}^2 \quad (5)$$

In the case of 2-NP, an overall reaction has been considered by lumping all the by-products, as shown in Eq. 6.

$$2\text{-}NP + (HO^{\bullet}\ or\ HOO^{\bullet}) \rightarrow products \quad (6)$$

In this regard, the disappearance of 2-NP can be modelled by Eq. 7.

$$-\frac{dC_{2\text{-}NP}}{dt} = C_{cat}\cdot k_{2\text{-}NP}\cdot C_{2\text{-}NP}\cdot C_{H_2O_2} \quad (7)$$

If a constant catalyst concentration is assumed, as well as the liquid volume, both H_2O_2 and 2-NP kinetic equations can be re-written as shown in Eqs. 8 and 9.

$$-\frac{dC_{H_2O_2}}{dt} = K_{H_2O_2,aq}\cdot C_{H_2O_2}^2 \quad (8)$$

$$-\frac{dC_{2\text{-}NP}}{dt} = K_{2\text{-}NP,aq}\cdot C_{2\text{-}NP}\cdot C_{H_2O_2} \quad (9)$$

where:

$$K_{H_2O_2,aq} = C_{cat}\cdot k_{H_2O_2} \quad (10)$$

$$K_{2\text{-}NP,aq} = C_{cat}\cdot k_{2\text{-}NP} \quad (11)$$

The kinetic model, summarized by Eqs. 8 and 9, was fitted to the experimental data obtained from each run with CNTs, resulting in the kinetic and statistical coefficients presented in Table 2.

The validation of this model is confirmed by the parity plot given in Fig. S2; it is also suitable according to the determination coefficients values obtained for the kinetic model employed in the experimental data obtained for each CNT ($R^2 > 0.953$). In addition, it is possible to observe that the model is able to reproduce accurately the experimental data through the simulated curves represented in Fig. 8.

The kinetic parameters (Table 2) obtained in the runs carried out with the CNTs show a correlation with the N-content of the samples (Fig. 9), just like previously observed with the conversions of 2-NP and H_2O_2. In this sense, the kinetic constant regarding the consumption of H_2O_2 ($K_{H2O2,aq}$) increased in the following order: E30 (2.51 $M^{-1}\,h^{-1}$) < A20E20 (3.16 $M^{-1}\,h^{-1}$) < E10A20 (4.29 $M^{-1}\,h^{-1}$) < A20E10 (7.44 $M^{-1}\,h^{-1}$) < A30 (40.0 $M^{-1}\,h^{-1}$). As observed, the material synthesized by feeding only acetonitrile (A30) shows a considerably higher kinetic constant compared to the other samples. The value determined for the kinetic constant of 2-NP oxidation ($K_{2\text{-}NP,aq}$) increases in the inverse order (with the exception of sample A30 that assumes the value of 3.70 $M^{-1}\,h^{-1}$): E30 (6.67 $M^{-1}\,h^{-1}$) > A20E20 (5.21 $M^{-1}\,h^{-1}$) > E10A20 (5.10 $M^{-1}\,h^{-1}$) > A20E10 (1.61 $M^{-1}\,h^{-1}$).

There are few works related to the CWPO of 2-NP and, to the best of our knowledge, there are no studies regarding the kinetic model of the CWPO of 2-NP to compare the results found in this work. However, similar kinetic power-law equations were applied previously in the modelling of CWPO of phenol with undoped and N-doped carbon black catalysts [8,9]. The kinetic constants regarding the disappearance of both H_2O_2 and phenol with the undoped material were 0.52 and 1.13 $M^{-1}\,h^{-1}$, respectively (recalculated considering the units and the catalyst load). The value of the kinetic constant increased upon N-doping of the carbon black, achieving 3.11 and 3.29 $M^{-1}\,h^{-1}$, for H_2O_2 and phenol disappearance constants, respectively [9]. Those values are lower when compared with those obtained in this work using CNTs, even taking into consideration that the CWPO of phenol was performed under more severe operating conditions (110 °C, C_{cat} = 5 g L^{-1}, $C_{Phenol,0}$ = 1 g L^{-1} and C_{H2O2} = 5 g L^{-1}) than those used in this study. Additionally, 2NP is expected to be harder to oxidize with hydrogen peroxide than phenol, according to other studies related to the oxidation of phenol and 2-NP [29–31].

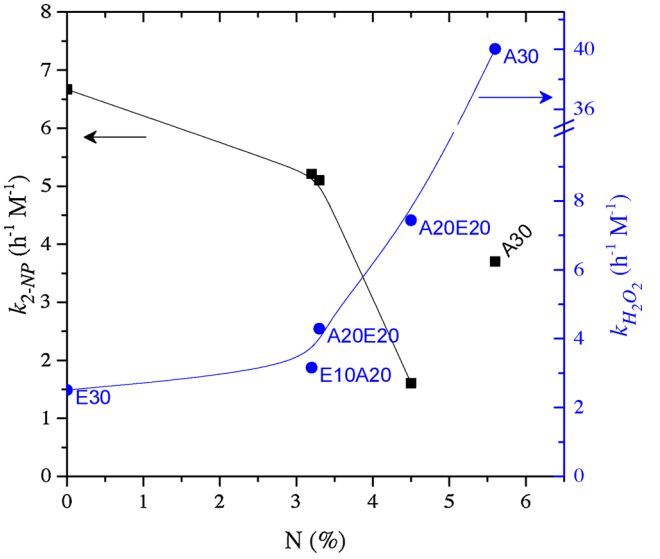

Fig. 9. Kinetic constants obtained employing the power-law kinetic model given by Eqs. 8 and 9 as a function of the nitrogen present in the CNTs.

3.4.2. CWPO of 2-NP in L-L biphasic mixtures

The decomposition of H_2O_2 was modelled in a way similar to that employed for the CWPO of 2-NP in aqueous phase runs (Eq. 5), since it is expected that H_2O_2 will remain in the aqueous phase during the biphasic CWPO runs. However, it is not possible to determine accurately the catalyst concentration in the decomposition of H_2O_2, since the entire surface of the catalyst is not expected to be in contact with the aqueous phase. Thus, the catalyst concentration was assumed to be constant, and Eq. 12 was used to model the consumption of H_2O_2, similar to Eq. 8 for the aqueous phase.

$$-\frac{dC_{H_2O_2}}{dt} = K_{H_2O_2,bip}\cdot C_{H_2O_2}^2 \quad (12)$$

The rate of disappearance of 2-NP in the oil phase can be described by the flux of compound from the oil phase to the aqueous phase, where the oxidation of 2-NP takes place. This mass transfer depends on the interfacial area ($A_{interface}$), the rate constant ($k_{2\text{-}NP,oil}$) and a driving force, that can be defined as the concentration difference of 2-NP in cyclohexane ($C_{2\text{-}NP,oil}$) and the equilibrium concentration of 2-NP ($C_{2\text{-}NP,oil,eq}$) between both the oil and water phases. Hence, the transfer rate of 2-NP can be described as shown in Eq. 13.

$$-\frac{dC_{2\text{-}NP,oil}}{dt} = A_{interface}\cdot k_{2\text{-}NP,oil}\cdot(C_{2\text{-}NP,oil} - C_{2\text{-}NP,oil,eq}) \quad (13)$$

The interfacial area was considered to be constant, and the

Table 2
Kinetic and statistical coefficients of 2-NP oxidation with H_2O_2 obtained for each CNT sample in aqueous solution (Eqs. 8 and 9) and emulsified biphasic mixture (Eqs. 14, 18 and 22).

Coefficient	E30	A20E20	E10A20	A20E10	A30
$K_{H_2O_2}$,aq ($M^{-1}\,h^{-1}$)	2.51	3.16	4.29	7.44	40.0
$K_{2\text{-}NP,aq}$ ($M^{-1}\,h^{-1}$)	6.67	5.21	5.10	1.61	3.70
SSE_{model}	0.033	0.058	0.042	0.035	0.021
R^2	0.977	0.953	0.959	0.971	0.990
$K_{H_2O_2}$,bip ($M^{-1}\,h^{-1}$)	0.000	0.041	0.050	0.080	0.258
$K_{2\text{-}NP,bip}$ ($M^{-1}\,h^{-1}$)	0.008	0.045	0.054	0.039	0.034
$K_{2\text{-}NP,oil}$ (h^{-1})	0.63	1.68	0.90	1.03	0.79
P_{OW}			32.4		
SSE_{model}	0.033	0.032	0.045	0.036	0.047
R^2	0.969	0.979	0.971	0.974	0.972

concentration of 2-NP in the equilibrium can be defined by the partition coefficient of 2-NP between oil and water (P_{OW}) and the concentration of 2-NP in the aqueous phase. Thus, Eq. 14 and 15 were taken into account to define the mass transfer of 2-NP from the oil to the aqueous phase, as described in Eq. 16.

$$A \cdot k_{2\text{-}NP,oil} = K_{2\text{-}NP,oil} \tag{14}$$

$$C_{2\text{-}NP,oil,eq} = P_{OW} \cdot C_{2\text{-}NP,aq} \tag{15}$$

$$-\frac{dC_{2\text{-}NP,oil}}{dt} = K_{2\text{-}NP,oil} \cdot (C_{2\text{-}NP,oil} - P_{OW} \cdot C_{2\text{-}NP,aq}) \tag{16}$$

This outflow of 2-NP from the oil phase is transferred as an inflow of 2-NP to the aqueous phase as described by Eq. 17.

$$\left(\frac{dC_{2\text{-}NP,aq}}{dt}\right)_{inflow} = K_{2\text{-}NP,aq} \cdot \left(\frac{C_{2\text{-}NP,oil}}{P_{OW}} - C_{2\text{-}NP,aq}\right) \tag{17}$$

Taking into account that the mass transfer must be equal between the phases (Eq. 16 and 17), the inflow of 2-NP in the aqueous phase can be defined as given in Eq. 18.

$$\left(\frac{dC_{2\text{-}NP,aq}}{dt}\right)_{inflow} = K_{2\text{-}NP,oil} \cdot (C_{2\text{-}NP,oil} - P_{OW} \cdot C_{2\text{-}NP,aq}) \tag{18}$$

On the other hand, the oxidation rate of 2-NP with hydrogen peroxide in the aqueous phase can be defined according to the previous Eq. 9, described for the CWPO of 2-NP. Assuming a constant catalyst load in contact with the aqueous phase, it is possible to describe the oxidation rate of 2-NP as shown in Eq. 19.

$$\left(-\frac{dC_{2\text{-}NP,aq}}{dt}\right)_{oxidation} = K_{2\text{-}NP,bip} \cdot C_{2\text{-}NP,aq} \cdot C_{H_2O_2} \tag{19}$$

Finally, the rate of disappearance of 2-NP in the aqueous phase was defined considering both contributions: (1) inflow of 2-NP from the oil phase (Eq. 18) and (2) oxidation rate of 2-NP (Eq. 19), resulting in Eq. 20.

$$\frac{dC_{2\text{-}NP,aq}}{dt} = K_{2\text{-}NP,oil} \cdot (C_{2\text{-}NP,oil} - P_{OW} \cdot C_{2\text{-}NP,aq}) - K_{2\text{-}NP,bip} \cdot C_{2\text{-}NP,aq} \cdot C_{H_2O_2} \tag{20}$$

The kinetic model, summarized by Eqs. 14, 18 and 22 was fitted to the experimental data obtained from each run with CNTs, resulting in the kinetic constants and statistical parameters presented in Table 2. The good fit of the kinetic model is represented by the parity plot given in Fig. S3, and by the coefficients of determination (higher than 0.969 for all runs performed with the CNTs). Then, the kinetic model is able to predict suitably the experimental data for the CNT-catalyzed runs (curves in Fig. 6). As expected, the highest kinetic constant regarding the decomposition rate of H_2O_2 ($K_{H2O2,bip}$) was obtained for sample A30 (0.258 $M^{-1}\,h^{-1}$), whereas a value close to zero was observed for E30. The Janus amphiphilic samples present values ranging from 0.041 to 0.080 $M^{-1}\,h^{-1}$, the highest value being observed for the sample A20E10. The kinetic constant related to the oxidation rate of 2-NP ($K_{2\text{-}NP,bip}$) presents the lowest value for the sample E30 (0.008 $M^{-1}\,h^{-1}$) and was 0.034 $M^{-1}\,h^{-1}$ for A30. The lowest value obtained with sample E30 can be ascribed to its lipophilic character, thus being preferentially distributed through the organic phase, decreasing the value of $K_{2\text{-}NP,bip}$, which depends on the concentration of the catalyst in the aqueous phase (Eq. 9, 21). For the Janus amphiphilic CNTs, the kinetic parameter was slightly higher than that obtained for A30, with values ranging from 0.039 to 0.054 $M^{-1}\,h^{-1}$. The material with the highest kinetic constant of 2-NP oxidation was E10A20. All values of the kinetic constants determined in the disappearance of both H_2O_2 and 2-NP in the biphasic mixture were significantly lower when compared with those in the CWPO of 2-NP in aqueous solution (Table 2). This means that the oxidation of 2-NP with H_2O_2 in the cyclohexane-water biphasic mixture is considerably slower than the CWPO of 2-NP, or that it is limited by the mass transfer of 2-NP from the oil to the aqueous phase. In this sense, the rate constant regarding the mass transfer of 2NP between the liquid phases ranges from 0.57 to 1.68 h^{-1}, yielding higher values (0.90-1.68 h^{-1}) when Janus amphiphilic materials (A20E20, E10A20 and A20E10) are used. This was ascribed to the increase of the interfacial area between phases, as a consequence of the Pickering emulsion stabilized by the CNTs. In order to compare the rate constants for the chemical oxidation and mass transfer of 2-NP, the kinetic model was modified considering that the concentration of H_2O_2 is in large excess compared to the concentration of 2-NP in the aqueous phase, thus being considered constant, yielding Eqs. 21 and 22.

$$K'_{2\text{-}NP} = K_{2\text{-}NP} \cdot C_{H_2O_2} \tag{21}$$

$$\frac{dC_{2\text{-}NP,aq}}{dt} = K_{2\text{-}NP,oil} \cdot (C_{2\text{-}NP,oil} - P_{OW} \cdot C_{2\text{-}NP,aq}) - K'_{2\text{-}NP} \cdot C_{2\text{-}NP,aq} \tag{22}$$

The disappearance rate of 2-NP defined by Eq. 22 was also found to predict suitably the experimental data (R^2 higher than 0.951), with the kinetic constant of the 2-NP oxidation ($K'_{2\text{-}NP}$) reaching values of 13.2, 50.9, 59.9, 33.4 and 14.2 h^{-1} for E30, A20E20, E10A20, A20E10 and A30, respectively. For the model given by Eq. 22, the rate constant of the 2-NP mass transfer ($K_{2\text{-}NP,oil}$) is 0.59, 1.39, 0.93, 0.60 and 0.51 h^{-1} for E30, A20E20, E10A20, A20E10 and A30, respectively. Both $K'_{2\text{-}NP}$ and $K_{2\text{-}NP,oil}$ constants, determined with the same units, can now be compared and, as observed, the mass transfer of 2-NP between phases is the rate-determining step of the process under the operating conditions considered. Both mass transfer and chemical oxidation rates improved after addition of the CNT catalysts, with $K_{2\text{-}NP,oil}$ increasing up to 1.39 and 0.93 h^{-1}, and $K'_{2\text{-}NP}$ increasing up to 50.9 and 59.9 h^{-1} for A20E20 and E10A20, respectively.

4. Conclusions

By feeding ethylene and acetonitrile precursors sequentially, catalytic chemical vapor deposition enables the synthesis of amphiphilic Janus-like carbon nanotubes (CNTs). The use of acetonitrile allows the synthesis of N-doped CNTs with a controlled quantity of nitrogen, by varying the feeding time and order of the precursors (ethylene for the undoped section and acetonitrile for the N-doped section of the materials). Consequently, the amphiphilic character of the materials can be tailored for specific applications.

The CNTs prepared in this study show catalytic activity in the CWPO of 2-NP, allowing a complete removal of the pollutant with the material prepared by feeding only ethylene (sample E30). A higher N-content on the materials, corresponding to a lower hydrophobic character, leads to a higher conversion of hydrogen peroxide and to a lower removal of 2-NP, as a consequence of parasitic reactions occurring due to high rates of hydrogen peroxide decomposition.

CNTs synthesized from both acetonitrile and ethylene precursors (A20E20, E10A20 and A20E10 samples) formed perfectly stable Pickering emulsions, due to their double structure (Janus-like form), obtained by sequentially feeding different precursors during their preparation. Furthermore, only the amphiphilic Janus-like materials (A20E20, E10A20 and A20E10) demonstrated significant catalytic activity in the removal of 2-NP with hydrogen peroxide in the simulated L-L biphasic mixture (cyclohexane-water). The activity can be attributed to the ability of these materials to form and stabilize Pickering emulsions, enhancing the contact between the catalyst and both phases, thus maximizing the interfacial area and ensuring a higher mass transfer between phases.

The disappearance rate of both H_2O_2 and 2-NP can be modelled suitably in the CWPO of 2-NP in aqueous phase, as well as in the oxidation of 2-NP in the biphasic mixture with H_2O_2, by employing second-order power-law kinetic equations. In the case of the biphasic system, the mass transfer of the pollutant between the phases must be taken into account. The model yielded higher kinetic constants after

introducing Janus-like CNTs and higher rate constants for the mass transfer of 2-NP between phases, which was ascribed to the capacity of the materials to stabilize the emulsion and to increase the interfacial area between the phases.

Acknowledgments

This work is a result of the Project “PLASTIC_TO_FUEL&MAT - Upcycling Waste Plastics into Fuel and Carbon Nanomaterials”, with the reference POCI-01-0145-FEDER-031439, supported by national funds through FCT and by the European Regional Development Fund (ERDF); the Project “AIProcMat@N2020 - Advanced Industrial Processes and Materials for a Sustainable Northern Region of Portugal 2020″, with the reference NORTE-01-0145-FEDER-000006, supported by Norte Portugal Regional Operational Programme (NORTE 2020), under the Portugal 2020 Partnership Agreement, through ERDF; and the Associate Laboratory LSRE-LCM - UID/EQU/50020/2019 - funded by national funds through FCT/MCTES (PIDDAC). Bruno F. Machado acknowledges the financial support of the exploratory project under the FCT Investigator Programme (ref. IF/00301/2015) with the financial support of FCT/MCTES through national funds (PIDDAC).

Appendix A. Supplementary data

Supplementary material related to this article can be found, in the online version, at doi:https://doi.org/10.1016/j.cattod.2019.07.012.

References

[1] A. Al-Futaisi, A. Jamrah, B. Yaghi, R. Taha, J. Hazard. Mater. 141 (2007) 557–564.
[2] C. Machín-Ramírez, A.I. Okoh, D. Morales, K. Mayolo-Deloisa, R. Quintero, M.R. Trejo-Hernández, Chemosphere 70 (2008) 737–744.
[3] G. Chen, G. He, Sep. Purif. Tech. 31 (2003) 83–89.
[4] L. Yu, M. Han, F. He, Arab. J. Chem. 10 (2017) S1913–S1922.
[5] A. Muniz, C. Dantas, A. Dantas Neto, M. Moura, Braz. J. Petrol. Gas. 6 (2012) 19–30.
[6] A.A.S. Oliveira, I.F. Teixeira, T. Christofani, J.C. Tristão, I.R. Guimarães, F.C.C. Moura, Appl. Catal. B 144 (2014) 144–151.
[7] J.L. Diaz de Tuesta, A.M. T. Silva, J.L. Faria, H. T. Gomes, Chem. Eng. J. 347 (2018) 963–971.
[8] J.L. Diaz de Tuesta, A. Quintanilla, J.A. Casas, J.J. Rodriguez, Appl. Catal. B 209 (2017) 701–710.
[9] J.L. Diaz de Tuesta, A. Quintanilla, J.A. Casas, J.J. Rodriguez, Catal. Commun. 102 (2017) 131–135.
[10] R.S. Ribeiro, A.M. T. Silva, J.L. Figueiredo, J.L. Faria, H. T. Gomes, Appl. Catal. B (140-141) (2013) 356–362.
[11] R.S. Ribeiro, A.M. T. Silva, M.T. Pinho, J.L. Figueiredo, J.L. Faria, H. T. Gomes, Catal. Today 240 (2015) 61–66.
[12] M. Martin-Martínez, R.S. Ribeiro, B. F. Machado, P. Serp, S. Morales-Torres, A.M. T. Silva, J.L. Figueiredo, J.L. Faria, H. T. Gomes, ChemCatChem 8 (2016) 2068–2078.
[13] F. Orshansky, N. Narkis, Water Res. 31 (1997) 391–398.
[14] A. Li, Q. Zhang, G. Zhang, J. Chen, Z. Fei, F. Liu, Chemosphere 47 (2002) 981–989.
[15] V. Kavitha, K. Palanivelu, J. Photochem. Photobiol. A Chem. 170 (2005) 83–95.
[16] M. Trapido, Y. Veressinina, J. Kallas, Ozone Sci. Eng. 23 (2001) 333–342.
[17] L. Keith, W. Telliard, Environ. Sci. Technol. 13 (1979) 416–423.
[18] Environmental Protection Agency, Nitrophenols, Ambient Water Quality Criteria, (1980), pp. A1–C134.
[19] M.H. Abraham, C.M. Du, J.A. Platts, J. Org. Chem. 65 (2000) 7114–7118.
[20] A.D. Purceno, B. F. Machado, A.P. Teixeira, T.V. Medeiros, A. Benyounes, J. Beausoleil, H.C. Menezes, Z.L. Cardeal, R.M. Lago, P. Serp, Nanoscale 7 (2015) 294–300.
[21] A. Perro, S. Reculusa, S. Ravaine, E. Bourgeat-Lami, E. Duguet, J. Mater. Chem. 15 (2005) 3745.
[22] Y. He, F. Wu, X. Sun, R. Li, Y. Guo, C. Li, L. Zhang, F. Xing, W. Wang, J. Gao, ACS Appl. Mater. Interfaces 5 (2013) 4843–4855.
[23] M. Tang, X. Wang, F. Wu, Y. Liu, S. Zhang, X. Pang, X. Li, H. Qiu, Carbon 71 (2014) 238–248.
[24] M. Pera-Titus, L. Leclercq, J.M. Clacens, F. De Campo, V. Nardello-Rataj, Angew. Chem. 54 (2015) 2006–2021.
[25] I.F. Teixeira, A.Ad.S. Oliveira, T. Christofani, F.C.C. Moura, J. Mater. Chem. A 1 (2013) 10203–10208.
[26] S. Brunauer, P.H. Emmett, E. Teller, J. Am. Chem. Soc. 60 (1938) 309–319.
[27] B.C. Lippens, J.H. de Boer, J. Catal. 4 (1965) 319–323.
[28] M. Thommes, K. Kaneko, A.V. Neimark, J.P. Olivier, F. Rodriguez-Reinoso, J. Rouquerol, K.S.W. Sing, Pure Appl. Chem. 87 (2015) 1051–1069.
[29] S. Chaliha, K.G. Bhattacharyya, Ind. Eng. Chem. Res. 47 (2008) 1370–1379.
[30] S. Chaliha, K. Bhattacharyya, Indian J. Chem. Technol. 13 (2006) 499–504.
[31] A. Santos, P. Yustos, S. Rodriguez, F. Garcia-Ochoa, Appl. Catal. B 65 (2006) 269–281.